Harvesting microalgal biomass using negatively charged polysulfone patterned membranes: Influence of pattern shapes and mechanism of fouling mitigation

Zhenyu Zhao, Koenraad Muylaert, Anthony Szymczyk, Ivo F J Vankelecom

Highlights

- Membrane charge and patterning significantly improve the membrane performance.
- Critical pressures of all sPSf blend patterned membranes were higher than 2.5 bar.
- Membrane with wave patterns showed the highest CWP and membrane flux.
- sPSf blend patterned membranes showed the lowest interaction energy.
- A higher velocity and wall shear were found on the pattern apexes.

Harvesting microalgal biomass using negatively charged polysulfone patterned membranes: influence of pattern shapes and mechanism of fouling mitigation

Zhenyu Zhao[a], Koenraad Muylaert[b], Anthony Szymczyk[c], Ivo F.J. Vankelecom[a]

[a]Membrane Technology Group (MTG), Division cMACS, Faculty of Bio-Science Engineering, KU Leuven, Celestijnenlaan 200F, PO Box 2454, 3001 Leuven, Belgium

[b]Lab Aquatic Biology, Microbial en Molecular Systems, KU Leuven KULAK, E. Sabbelaan 53, B-8500 Kortrijk, Belgium

[c]Université de Rennes 1, Institut des Sciences Chimiques de Rennes, UMR CNRS 6226, 263 Avenue du Ge'ral Leclerc, 35042 Rennes, cedex, France

Abstract:

Membranes have a lot of potential for harvesting microalgae, but membrane fouling is hampering their breakthrough. In this study, the effects of charge and corrugated surface on membrane filtration performance were investigated. The clean water permeance (CWP), the microalgae harvesting efficiency and the membrane flux for a microalgal broth were determined using patterned polysulfone (PSf) membranes with different shapes of the surface patterns and containing different charge densities by blending sulfonated polysulfone (sPSf). The flow behavior near the patterned membrane surface, as well as the interaction energy between membrane and microalgae were investigated using computational fluid dynamics (CFD) simulation and the improved extended "Derjaguin, Landau, Verwey, Overbeek" (XDLVO) theory, respectively. Membrane charge and pattern shape significantly improve the membrane

performance. The critical pressures of all sPSf blend patterned membranes were higher than 2.5 bar. A 4.5w% sPSf blend patterned membranes with wave patterns showed the highest CWP (2300 L/m^2 h bar) and membrane flux in the microalgal broth (1000 L/m^2 h bar) with 100% harvesting efficiency. XDLVO analysis showed that sPSf blend patterned membranes prepared obtained the lowest interaction energy and highest energy barrier for microalgal attachment. CFD simulation showed a higher velocity and wall shear on the pattern apexes.

Key words: Patterned membrane; Computational fluid dynamics; Cross-flow filtration; XDLVO; Interaction energy; Membrane technology; Membrane development

1. Introduction

Microalgae have gained increasing attention due to their fast growth rate, high CO_2 fixation rate and content of bio-active compounds (Chen et al., 2020; Suparmaniam et al., 2019; Zhao et al., 2018; Zhao et al., 2020e). Moreover, microalgae can use a variety of waste components as nutrients to produce high-value products and treat wastewater (Li et al., 2016; Shahid et al., 2020; Zhao et al., 2016b). For further commercialization purposes, technologies are required to reach high microalgal biomass concentrations at low cost and high efficiency. However, harvesting microalgae still remains a problem, because of the small size of the microalgal cells, the high dilution of cells in the broth and the high energy required for conventional harvesting via centrifugation (Zhao et al., 2020c; Zhao et al., 2020d). Membrane filtration processes have been seen as an alternative to harvest microalgae, due to their

high microalgae retention, high harvesting efficiency, ease of upscaling and low energy input (Bilad et al., 2012b; Zhao et al., 2020d). A membrane with high flux, high microalgal cell retention and low fouling propensity is the prerequisite to harvest microalgae. However, membrane fouling is always inevitable, which directly lowers membrane flux and requires frequent cleaning cycles. The latter lowers membrane life-time and increases operational costs while creating waste streams (Bilad et al., 2012a; Zhao et al., 2020d).

Increasing the hydrophilicity of the membranes and introducing surface charge are commonly used approaches to prevent fouling (Bilad et al., 2012a; Marbelia et al., 2016a). The adhesion forces between the membrane surface and water increase with increasing membrane hydrophilicity, resulting in a strong adsorbed layer of water molecules on the membrane surface. As a result, less attachment is found between the foulant and membrane surface (Zhu and Jun Loh, 2015). Introducing surface charge is an efficient approach to eliminate charged foulants. When the membrane surface and the foulants have similar charge, electrostatic repulsion can prevent the foulants from attaching to the surface, therefore mitigating fouling and enhancing membrane fluxes (Zhong et al., 2012). The foulants in a microalgal broth mainly come from microalgal cells and extracellular organic matter (EOM). Their charge is normally negative, mainly due to sulphated extracellular polysaccharides, carboxylic acids, uronic acids or acidic sugars on the cell surface and suspended in the broth (Marbelia et al., 2016b; Zaouk et al., 2018). A membrane with higher hydrophilicity and negative charge may thus present a better anti-fouling performance and higher membrane fluxes. A

negatively charged polycarbonate (PC) membrane has thus been used to harvest *Chlorella vulgris* (*C. vulgris)*, showing higher hydrophilicity, microalgal retention and membrane flux (Huang et al., 2020). A negatively charged polyacrylonitrile membrane was used to harvest eight types of microalgae, also showing higher water permeances and less fouling (Marbelia et al., 2016b). Sulfonated polysulfone (sPSf) has been incorporated into membranes to successfully create negative charges and a higher hydrophilicity (Song et al., 2016; Zhao et al., 2020a; Zhao et al., 2021).

The physico-chemical interaction between membrane surface and foulants in an aqueous solution can normally be revealed using the extended Derjaguin, Landau, Verwey, Overbeek (XDLVO) theory which contains the attractive Lifshitz-van der Waals (LW), Lewis acid-base (AB) and electrostatic repulsive double layer (EL) interactions (Hoek and Agarwal, 2006; van Oss, 1993). However, this theory can only be used to quantitatively calculate the interaction energy between two infinitely flat surfaces. Many microalgal shapes are spherical or elongated, and many membrane surfaces are rough and/or patterned (Lin et al., 2014; Marbelia et al., 2016b). An improved theory, the Derjaguin approximation, has been developed to quantitatively deal with the physico-chemical interactions between a spherical microalgal cell and a flat membrane surface (Wang et al., 2014). The interactions between polyvinylidene fluoride (PVDF)/polyethersulfone membranes and microalgae/extracellular organic matter (EOM) have been successfully characterized (Zhao et al., 2016a), but the interaction between sPSf blend membranes and microalgal cells is still unknown.

In addition to the hydrophilicity and surface charge modifications, surface

patterning is considered an emerging method to alleviate fouling due to the unique hydrodynamic flow behavior near the membrane surface and the extended active area (Ilyas et al., 2020; Jung and Ahn, 2019; Marbelia et al., 2020; Zhao et al., 2020b). Patterned membranes have been used for waste water treatment and microalgae harvesting, showing higher membrane fluxes than corresponding flat membranes (Lee et al., 2013; Zhao et al., 2020b; Zhao et al., 2021). The traditional ways for modifying the membrane surface are template-based molding, direct printing (e.g. 3-D printing and etching) and chemical modification (Heinz et al., 2018), which are always limited by equipment/mold cost, complex parameter control, compressed porosity and/or low pattern fidelity (Ma et al., 2015; Marbelia et al., 2020). A recently reported one-step method, phase inversion (Hołda and Vankelecom, 2015) by spraying using corrugated casting knives, may solve these problems (Marbelia et al., 2020). The polymer solution is cast using a modified patterned knife, and non-solvent is simultaneously sprayed on the cast film to rapidly solidify the surface pattern. The membrane prepared using this modified phase inversion method showed a significantly higher clean water permeance (CWP) than when using the traditional phase inversion method (Ilyas et al., 2020; Marbelia et al., 2020; Zhao et al., 2020b). The anti-fouling property of the patterned membrane is highly related to the pattern shape (Choi et al., 2017). However, current studies only focus on one kind of pattern shape, the comparison between different pattern shapes still needs to be further investigated.

In this study, sPSf was used to create negative charges on PSf membranes. The comparison of membranes with different pattern shapes for microalgae harvesting was

investigated. The one-step method, phase inversion by spraying, was used to prepare membranes with patterns at their active side. The interaction energies between microalgal cells and the membrane surface were calculated to unravel the mechanism governing the foulant deposition and release in the cross-flow system. The fluid behavior near the membrane surface in a cross-flow system was analyzed using computational fluid dynamics (CFD).

2. Materials and methods

2.1 Microalgae cultivation

Desmodesmus sp. (Zhao et al., 2020e) was cultivated in a 30 L plexiglas column photobioreactor with 25-L BG-11 medium (Zhao et al., 2016b). The cultivation was under continuous illumination with a light intensity of 100 μmol photons m^{-2} s^{-1}. Continuous aeration was kept constant at a rate of 15 L/min. After 10 days of cultivation, 10 mL microalgae broth was filtrated through a 0.1 μm filter to remove the cultivation medium and salts. The filter with microalgal paste was put in an oven under 105 °C until constant weight. The final dry weight of the microalgae was 0.88±0.02 g/L.

2.2 sPSf synthesis and characterization

sPSf was synthesized using direct sulfonation according to a previous study (Manea and Mulder, 2002). Briefly, PSf (25 g) (Solvay, Udel P-1700, Belgium) was completely dissolved in 300 mL of chloroform (Sigma-Aldrich, Belgium). A 10 mL 6M chlorosulfonic acid (99%, Sigma-Aldrich, Belgium) solution was prepared in chloroform and was then added dropwise to the PSf solution while stirring vigorously

for 1 h at 0 °C until a viscous precipitate was formed. The supernatant was then removed. The precipitate was washed first using chloroform and then with deionized water until neutral pH. After drying in a vacuum oven for 4 days at 40 °C, sPSf powder was obtained.

The degree of sulfonation (DS) and the ion-exchange capacity (IEC) of the obtained sPSf powder were determined using the back-titration method (Manea and Mulder, 2002; Song et al., 2016). sPSf powder (0.1 g) was soaked in a 1 M H_2SO_4 solution for 24 h, then washed using deionized water until neutral pH, and soaked into a 3 M NaCl solution for another 24 h. The NaCl solution was then titrated using a 0.01 M NaOH solution, and using phenolphthalein (5%, Sigma-Aldrich, Belgium) as indicator. The DS and IEC were calculated as follows:

$$DS\ (\%) = \frac{0.442cv}{M-0.08cv} \times 100\% \quad (1)$$

$$IEC\ (meq/g) = \frac{1000DS}{442+81DS} \quad (2)$$

where *c* is the concentration of NaOH solution (M), *v* the reacted volume of NaOH solution (mL), *M* the mass of sPSf (g).

2.3 Membrane preparation

Patterned membranes were prepared using four different patterned knives (with a wave, triangle, rectangle or trapezoid pattern) and a spray-modified non-solvent induced phase separation (s-NIPS) method according to a previous study (Marbelia et al., 2020). Patterned knives were 3D printed using VeroWhitePlusTM RGD835 (Stratasys Ltd, Eden Prairie, USA) as resin material with constant pattern height (h) of 1000 μm and inter-pattern distance (d) of 2000 μm (Fig. 1a). PSf (13.5w%), sPSf

(4.5w%) and deionized water (1w%) were dissolved in N-methyl-2-pyrrolidone (99w%, Acros organics, Belgium) at 60 °C with 25w% polyethylene glycol (PEG, Mw~1000 Da, Fluka, Belgium) as pore-forming agent (Zhao et al., 2020b; Zhao et al., 2021). After degassing overnight, the solution was cast on a smooth glass plate with a wet thickness of 200 μm (measured from the valley point of the corrugation to the bottom of the polymer film, below referred to as base-layer) at a casting speed of 2.3 cm/s. Deionized water as non-solvent was sprayed on the cast film simultaneous with the move of the casting knife in order to rapidly initiate the phase inversion process and fix the patterns (Hołda and Vankelecom, 2015; Marbelia et al., 2020). The cast film was immediately immersed into deionized water (20 °C) to complete the phase inversion (Hołda and Vankelecom, 2015). Four different patterned membranes were referred to as Wave, Tri, Rec and Trap, respectively (Fig. 1). To investigate the effect of sPSf and s-NIPS on membrane performance and properties, three different non-patterned membranes were prepared with the same wet thickness using a conventional casting knife: (1) one prepared using the s-NIPS method and a casting solution with 13.5w% PSf, 4.5% sPSf (total polymer concentration of 18w%), 25w% PEG and 1w% deionized water; (2) one prepared using the conventional non-solvent induced phase separation (NIPS, i.e. by directly immersing the cast film into the coagulation bath without any spraying) using a casting solution with 13.5w% PSf, 4.5% sPSf, 25w% PEG and 1w% deionized water; (3) one uncharged reference membrane prepared using the conventional NIPS method and a casting solution with 18w% PSf,

25w% PEG and 1w% deionized water. These three flat (F) membranes were referred as F-sNIPS, F-NIPS and F-PSf, respectively.

The casting solutions of all patterned membranes, F-sNIPS and F-NIPS membranes are the same. All patterned membranes and F-sNIPS membrane were prepared using the s-NIPS method, while F-NIPS and F-PSf membranes were prepared using the conventional NIPS method.

2.4 Analytical methods

The actual pattern height (H) and inter-pattern distance (D), the base-layer thickness (B) (Fig. 1b), and the cross-sections of patterned membranes were determined and observed using scanning electron microscopy (SEM, JEOL JFC-1300, Tokyo, Japan)..

The contact angles of three probe liquids (MiliQ water, glycerol and diiodomethane) were determined using a contact angle goniometer (Kruss, Drop Shape Analysis System, Germany). The hydrophilicity of the membrane was characterized using the contact angle measured with MiliQ water. A higher surface tension (lower MiliQ water contact angle) corresponds to a more hydrophilic surface (Dobrak-Van Berlo et al., 2011).

The membrane surface chemical composition was characterized using attenuated total reflectance Fourier-transform infrared spectrometer (ATR-FTIR, Bruker Alpha, Germany) with 4000-400 cm^{-1} scanning range.

The zeta potential (ZP) of the membrane surface was determined by streaming current measurements using an adjustable-gap measuring cell (SurPASS

Electrokinetic Analyzer, AntonPaar), following the procedure described before (Marbelia et al., 2016b). Visiolab software was used for data analysis.

Because the surface geometry may influence the measured results, three different flat membranes (F-sPIS, F-NIPS and F-PSf) were used. The property of F-sPIS can reflect the properties of patterned membranes.

The size and morphology of *Desmodesmus* sp. were determined and observed using an inverted microscope operated through CellSens (IX83, Olympus Corporation, Japan).

The ZP of *Desmodesmus* sp. was determined using a Nanobrook Omni Zeta Potential Analyzer (Brookhaven Corporate Park, Holtsville, USA), following the procedure described before (Marbelia et al., 2016b). Microalgal ZP was calculated using the Smoluchowski equation.

To determine the contact angle of *Desmodesmus* sp., fresh mciroalgal broth was filtrated through an F-PSf membrane. The retained microalgae paste on the membrane surface was pressed to form a flat film. The resulted microalgal flat film was then dried at ambient temperature for 24 h to remove surplus water. The microalgal contact angle was also determined using contact angle goniometer and three probe liquids.

2.5 Filtration experiment

2.5.1 Dead-end filtration

Membrane fluxes (J_m) of different membranes were determined using a high-throughput dead-end filtration system (HTML, Belgium) (Vandezande et al., 2009) containing 16 membrane coupons with a 1.77 cm^2 filtration active area each.

Before filtrating the microalgal broth, the membrane was first stabilized using deionized water at 1 bar for 20 min to stabilize the membrane. Membrane flux was measured using microalgal broth as the feed under 0.5 bar pressure for 10 min, and was calculated using Eq. (1). The CWP was measured using deionized water as feed. The optical density (OD) was determined to calculate microalgae harvesting efficiency (*E*) using a spectrophotometer (UV-1800, SHIMADZU, Belgium) at 680 nm and was calculated using Eq. (2).

$$J_m(L/m^2\ h\ bar) = \frac{V}{A \cdot t \cdot TMP} \qquad (1)$$

$$E\ (\%) = \frac{OD_f - OD_p}{OD_f} \qquad (2)$$

where A is the membrane active area (m^2); t the filtration time (h); TMP the trans-membrane pressure (bar); OD_f the absorbance of the feed; OD_p the absorbance of the permeate.

2.5.2 Cross-flow filtration

The filtration performances of different membranes were determined using a pressure-driven HT cross-flow filtration system (HTML, Belgium) which contains 4 membrane samples with 10 cm^2 filtration active area each, and microalgal broth was used as feed. Before filtrating the microalgal broth, the membrane was first stabilized using deionized water with a maximum pump speed of 0.015 m/s at 2.5 bar for 6 h until the CWP leveled off. The patterned membranes were fixed with the pattern lines perpendicular to the flow direction. The critical pressure (CP, bar) was determined using a stepwise method (Bilad et al., 2012a; Zhao et al., 2020b). Briefly, the filtration was carried out at a cross-flow velocity of 0.015 m/s and initialized under a pressure

of 1 bar. After every 2 h, the pressure was increased by 0.5 bar until the maximum pressure of 2.5 bar.

The Reynolds number (*Re*) of the feed flow in the cross-flow system was calculated using Eq. (3) with a known broth density of around 1024 kg/m^3 and an apparent viscosity of 0.0018 Pa/s (Michels et al., 2010).

$$Re = \frac{\rho v r}{\mu} \qquad (3)$$

where ρ is the broth density (kg/m^3); v the cross-flow velocity (m/s); r the inner diameter of the tube (m); μ the apparent viscosity (Pa/s).

2.6 CFD modeling

Flow behavior near the surface of the different membranes was simulated using a commercial fluid dynamics software (Ansys 19.0, Ansys Inc., USA). The colored areas and path lines represent the distribution of velocity and flow direction. Wall shear on the membrane surface was expressed using single colored lines.

2.7 Statistic analysis

All experiments were carried out three times, and the results were expressed as mean values±standard deviation. The significance of the results was analyzed using statistical product and service solutions (SPSS) 17.0 and analysis of variance (ANOVA) with least significant digit (LSD) analysis (P<0.05).

2.8 Interaction energy calculation

Considering that the surface energy and interfacial forces between the membrane surface and microalgae are related to the membrane and microalgae intrinsic properties, only F-sNIPS, F-NIPS and F-PSf membranes were used for calculation.

F-sNIPS membrane was prepared using the same casting solution and phase inversion method as for the patterned membranes, which can be used to reflect the patterned membranes surface properties.

The total interaction energy (ΔG^{Tot}, mJ/m^2) between the membrane surface and microalgae cells in the medium, including LW (ΔG^{LW}, mJ/m^2), EL (ΔG^{EL}, mJ/m^2) and AB (ΔG^{AB}, mJ/m^2) interactions (Hoek and Agarwal, 2006), can be expressed as the XDLVO interaction energy per unit area between two infinite planar surfaces using Eqs. (4)-(7) (Wang et al., 2014).

$$\Delta G^{Tot} = \Delta G^{LW} + \Delta G^{EL} + \Delta G^{AB} \quad (4)$$

$$\Delta G^{LW} = -\frac{A_L}{12\pi l^2} \quad (5)$$

$$\Delta G^{EL} = \varepsilon\varepsilon_0\kappa\zeta_A\zeta_M\left[\frac{\zeta_A^2+\zeta_M^2}{2\zeta_A\zeta_M}\left[1-\coth(\kappa l)\right]+\frac{1}{\sinh(\kappa l)}\right] \quad (6)$$

$$\Delta G^{AB} = \Delta G_{l_0}^{AB}\exp\left(\frac{l_0-l}{\lambda}\right) \quad (7)$$

where l is the separation distance between two infinite planar surfaces (l_0 is the minimum separation distance); A_L ($= 12\pi l_0^2\,\Delta G_{l_0}^{LW}$) the Hamaker constant; ε (78.5) and ε_0 (8.854×10^{-2} CV^{-1}/m) the dielectric constant of water and the dielectric permittivity of the vacuum, respectively (Zhao et al., 2016a); κ, the inverse Debye length, calculated using Eq. (8) (Ahmad et al., 2013; Gojkovic et al., 2020; Wang et al., 2014); ζ_A and ζ_M are the microalgae and membrane surface ZPs, respectively; λ (0.6 nm) the decay length of AB interaction in aqueous solution (Lin et al., 2014); $\Delta G_{l_0}^{LW}$, $\Delta G_{l_0}^{EL}$ and $\Delta G_{l_0}^{AB}$ are three interaction components at the minimum separation distance for two planar surfaces, which can be calculated using Eqs. (9)-(11).

$$\kappa = \sqrt{\frac{e^2 \sum n_i z_i^2}{\varepsilon \varepsilon_0 KT}} \quad (8)$$

$$\Delta G_{l_0}^{LW} = -2(\sqrt{\gamma_M^{LW}} - \sqrt{\gamma_W^{LW}})(\sqrt{\gamma_A^{LW}} - \sqrt{\gamma_W^{LW}}) \quad (9)$$

$$\Delta G_{l_0}^{EL} = \frac{\varepsilon \varepsilon_0 \kappa}{2}(\zeta_A^2 + \zeta_M^2)[1 - \coth(\kappa l_0) + \frac{2\zeta_A \zeta_M}{\zeta_A^2 + \zeta_M^2}\operatorname{csch}(\kappa l_0)] \quad (10)$$

$$\Delta G_{l_0}^{AB} = 2[\sqrt{\gamma_W^+}\left(\sqrt{\gamma_A^-} + \sqrt{\gamma_M^-} - \sqrt{\gamma_W^-}\right) + \sqrt{\gamma_W^-}\left(\sqrt{\gamma_A^+} + \sqrt{\gamma_M^+} - \sqrt{\gamma_W^+}\right) - \sqrt{\gamma_A^- \gamma_M^+} - \sqrt{\gamma_A^+ \gamma_M^-}] \quad (11)$$

where the subscripts *A*, *W* and *M* represent microalgae, water and membrane, respectively; γ the surface tension parameter; γ^{LW}, γ^+ and γ^- the LW component, electron-acceptor and electron-donor parameters, respectively; *T* the absolute temperature; *e* the electron charge; n_i the number concentration of ion *i* in microalgal broth; z_i the valence of ion *i*; *K* the Boltzmann's constant.

To calculate three energy components (LW, EL and AB), the surface tension parameters/components (γ) should be determined. The total tension parameter (γ^{Tot}), including LW (γ^{LW}) and AB (γ^{AB}) components (Van Oss et al., 1986), can be calculated using Eq. (12), which can also be calculated using the extended Young equation (EYE) by testing the contact angle using three probe liquids (Li et al., 2014). The EYE can be expressed as Eq. (13) (Huang et al., 2014):

$$\gamma^{Tot} = \gamma^{LW} + \gamma^{AB} \quad (12)$$

$$(1 + \cos\theta)\gamma_L^{Tot} = 2(\sqrt{\gamma_S^{LW}\gamma_L^{LW}} + \sqrt{\gamma_S^+ \gamma_L^-} + \sqrt{\gamma_S^- \gamma_L^+}) \quad (13)$$

$$\gamma^{AB} = 2\sqrt{\gamma^- \gamma^+} \quad (14)$$

where the subscripts *S* and *L* represent the solid (i.e. membrane and microalgae) surface and the liquid, respectively.

Eqs. (9)-(11) can only allow for two planar surfaces, while *Desmodesmus* sp. is

spherical according to the microscope observation, and the cell size ranges from 5.1-7.0 μm. The Derjaguin approximation (DA) was thus used to calculate the interaction energy components ($U_{sph}^{LW}(l)$, $U_{sph}^{EL}(l)$ and $U_{sph}^{AB}(l)$) between a spherical surface (mciroalgal cell) and planar surface (membrane) (Derjaguin, 1934). The calculation can be expressed using Eqs. (15)-(18). $U_{sph}^{LW}(l_0)$, $U_{sph}^{EL}(l_0)$ and $U_{sph}^{AB}(l_0)$ represent three interaction energy components at the minimum separation distance for spherical and planar surfaces.

$$U_{sph}^{Tot}(l) = U_{sph}^{LW}(l) + U_{sph}^{EL}(l) + U_{sph}^{AB}(l) \quad (15)$$

$$U_{sph}^{LW}(l) = 2\pi\Delta G_{l_0}^{LW} \frac{l_0^2 a_A}{l} \quad (16)$$

$$U_{sph}^{EL}(l) = \pi\varepsilon\varepsilon_0 a_A \left[2\zeta_A\zeta_M \ln\left(\frac{1+e^{-\kappa l}}{1-e^{-\kappa l}}\right) + (\zeta_A^2 + \zeta_M^2)\ln(1-e^{-2\kappa l})\right] \quad (17)$$

$$U_{sph}^{AB}(l) = 2\pi a_A \lambda\Delta G_{l_0}^{AB} \exp\left(\frac{l_0 - l}{\lambda}\right) \quad (18)$$

where $U_{sph}^{Tot}(l)$ is the modified total interaction energy; a_A the mciroalgal cell radius.

3. Results and discussion

3.1 Characterization of membranes and microalgae

The DS and IEC of the resulting sPSf in current study are 71% and 1.4 meq/g, respectively, indicating a high degree of sulfonation and a relatively high hydrophilicity (Song et al., 2016). sPSf with 71% DS is not water-soluble, preventing sPSf from leaching out from the membrane during phase inversion and filtration. To verify the successful incorporation of sPSf in membranes, FTIR was used. The spectrum (Fig. 2) shows a small characteristic peak at ~1041 cm^{-1}, which corresponds to the symmetric stretch vibration of the S=O bond in the sulfonic acid group, indicating the successful incorporation of sPSf in the blend membrane.

The cross-sectional morphologies of the patterned membranes are shown in Fig. 3, showing a typical asymmetric structure with finger-like macrovoids with a remarkable triple-layered structure. The dense skin layer is thicker in the valley than at the apex (Fig. 3), indicating that the fluxes at the apex may be higher than in the valley. The possible reason is that the phase inversion process in the valleys is different from that at the apex as out-diffusing solvent mixes with a smaller amount of non-solvent, which is present and stagnant in the valley than on top of the patterns (Fig. 4). As the spraying nozzle covers a width of around 6 cm, and the volume of sprayed water is 3.6 mL/s at a casting speed of 2.5 cm/s. The theoretical corresponding sprayed non-solvent thickness is then about 660 μm (assuming a flat surface). This amount of water is enough for the initial solidification. However, as the volume of water in the valley is less than on the apex, the skin layer properties change along the exact position on the waves (Hołda and Vankelecom, 2015). A similar result was found in a previous study(Zhao et al., 2020b).

After introducing sPSf into the membrane, the membrane surface hydrophilicity and negative charge increased significantly (Table 1) (i.e. the water contact angles and ZPs of the F-sNIPS and F-NIPS membranes were lower than those of the F-PSf membrane), indicating the antifouling potential for microalgae harvesting.

Interfacial Gibbs free energies at a minimum separation distance between membrane surface and microalgal cells were calculated based on the surface tension data from Table1 and are shown in Table 2. The contribution of EL free energy is normally a magnitude lower than that of LW and AB free energies and can be

considered as negligible (Cao et al., 2015; Zhao et al., 2016a). The total interfacial Gibbs free energy ($\Delta G_{l_0}^{Tot}$) was therefore calculated by the sum of $\Delta G_{l_0}^{LW}$ and $\Delta G_{l_0}^{AB}$. A negative value of $\Delta G_{l_0}^{Tot}$ represents an attractive interaction, on the contrary a repulsive interaction (Li et al., 2014). In addition, a higher absolute value of $\Delta G_{l_0}^{Tot}$ means a higher attractive strength between two surface (Li et al., 2014). From Table 2, negative values of $\Delta G_{l_0}^{Tot}$ indicate an attractive interaction between membrane and microalgal cells as well as microalgal cells themselves. The most negative value is found between microalgal cells (-67.7), indicating that microalgal cells tend to aggregate more and create fouling. By adding sPSf and using the s-NIPS method, the lowest negative value of $\Delta G_{l_0}^{Tot}$ is found between F-sNIPS membrane and microalgal cells (-33.6), indicating an alleviated membrane fouling. The surface property of F-sPIS can be approximately considered as the same as for patterned membranes made from the same casting solutions and the s-NIPS method, indicating reduced fouling even though without unique flow behavior on the patterned membrane surface.

3.2 Effect of the pattern shape on membrane performance

To investigate the effects of pattern shape, the membranes were prepared using four different patterned knives (wave, triangle, rectangle and trapezoid) with fixed PSf, sPSf, PEG and deionized water concentrations of 13.5w%, 4.5w%, 25w% and 1w% in the membrane casting solutions, respectively. Three flat membranes (F-sNIPS, F-NIPS and F-PSf) with the same wet casting thickness were prepared for comparison. Membranes were first potted in a dead-end filtration system to determine the CWP

and the membrane flux in a microalgal broth (Fig. 5). The patterned membranes were more water-permeable compared with the flat membranes (Fig. 5a), in line with previous studies (Marbelia et al., 2020; Zhao et al., 2020b; Zhao et al., 2021). The flat membranes prepared by adding 4.5w% sPSF showed a higher CWP. Incorporation of sPSf improves the affinity between water and the membrane surface (i.e. higher hydrophilicity, Table 1) by creating more hydrogen bonds and enhancing polar interactions (Luo et al., 2017). In addition, the porosity, mean pore size and hydrophilicity also increase, therefore facilitating transport of water (Song et al., 2016; Zhao et al., 2020a; Zhao et al., 2021). The CWP of the F-sNIPS membrane was significantly (P<0.05) higher than that of F-NIPS, indicating that mere use of the s-NIPS method did increase the membrane permeability. Similar results were explained in a previous study (Marbelia et al., 2020). All these results showed that the high CWP of the patterned membrane was not only caused by the extended surface area and the introduction of charges, but can also be partly intrinsically ascribed to the s-NIPS method.

A similar trend was found when harvesting microalgae (Fig. 5b). The harvesting efficiency of each membrane was higher than 99%, validating the feasibility of harvesting microalgal biomass. Interestingly, while the CWPs of F-NIPS and F-PSf had no significant difference (P>0.05), the membrane fluxes of these two membranes in the microalgal broth showed significant differences (P<0.05). This can be linked to the fact that most of the microalgal cells are surrounded by carboxylic acids, uronic acids or acidic sugars, hence carrying negative charges that are rejected by the

membrane surface charge (Marbelia et al., 2016b; Zhao et al., 2020a). Membrane flux can thus effectively be enhanced when less microalgal cells and/or EOM deposit on the membrane surface. For the patterned membranes, the Wave-membrane showed the highest CWP and membrane flux in the microalgal broth, followed by the Tri, Trap and Rec membranes. The patterned and flat membranes were potted in a cross-flow filtration system to investigate the effect of pattern shape on filtration performance (Fig. 6). The anti-fouling property of each membrane was evaluated using CP. With step-wise increasing the pressure, the fouling on the membrane surface became more significant. A higher CP therefore represents a higher anti-fouling capacity. The experimental limit was at 2.5 bar. Compared with the F-PSf membrane (CP=2.5 bar), all other membranes showed a CP higher than 2.5 bar, thus proving the efficiency of incorporating sPSf as anti-fouling strategy. The filtration curves of Tri and Trap membranes almost overlap, which is in line with the results in the dead-end filtration system. These two shapes thus rendered similar filtration performance. The filtration curves of all patterned membranes are situated above those of the flat membranes. Even after 8-h filtration, they still can give a relatively high membrane flux. For the patterned membranes, more microalgal cells were deposited in the valley regions rather than on the ridges, probably due to the enhanced wall shear on the ridge regions or the different local fluxes (Marbelia et al., 2020; Maruf et al., 2014; Zhao et al., 2020b). For the flat membranes, the cake layer can easily cover the whole membrane surface due to the constant flow behavior on the membrane (Zhao et al., 2020b; Zhao et al., 2021). The filtration curve of the

Wave-membrane is situated above that of the other membranes, indicating that the wave shape does significantly improve the filtration performance.

These numbers are all much higher than in literature, even though broth conditions will surely be slightly different. A flat PSf membrane used in the cross-flow system for *C. pyrenoidosa* harvesting, showed a maximum CWP of 270 L/m^2 h bar and a broth flux of 92 L/m^2 h bar (Sun et al., 2014). A negatively charged PC membrane was used for *C. vulgaris* harvesting, showing a maximum membrane flux in a microalgal broth of 133 L/m^2 h bar (Huang et al., 2020). A recent study using flat PVDF membranes without surface pattern in tilted panel and axial vibration systems to harvest *Euglena* sp. and *C. pyrenoidosa* showed membrane permeances of 724 and 640 L/m^2 h bar, respectively (Lau et al., 2020; Zhao et al., 2016a). Even with enhanced shear near the membrane surface (i.e. 14512 s^{-1}) and lower microalgal concentration (i.e. 0.6 g/L of *Euglena* sp. and 0.55 g/L of *C. pyrenoidosa*), the membrane permeances were still much lower than those reported here using negatively charged membranes with a wave pattern. All negatively charged patterned membranes in current study showed a significantly higher membrane permeance in both microalgal broth (up to 1000 L/m^2 h bar) and CWP (up to 2250 L/m^2 h bar), indicating an important advantage of the synergy between surface charge and pattern. A previous study using negatively charged PSf patterned membrane to harvest *C. vulgaris* also showed a huge improvement in membrane flux upon charge creation (Zhao et al., 2021).

3.3 Interaction energy analysis

The profiles of interaction energies between microalgal cells and three flat membranes as a function of the separation distance are shown in Fig. 7. A positive value represents a repulsive energy; a negative value an attractive energy. The interaction energy curves of F-sNIPS and F-NIPS almost overlap, indicating a similar interaction energy with microagal cells for these two membranes, as could be expected. This confirms that phase inversion does not change the membrane surface property. With decreasing the distance between microalgal cells and membrane surface, repulsive electrostatic and attractive Van der Waals energies all increase (Figs. 7b and 7d). The total interaction energy profile shows an actual microalgal adhesion energy barrier on the membrane surface that the microalgal cells must overcome an energy barrier (Wang et al., 2014). Therefore, a higher repulsive energy barrier represents that only a small part of microalgal cells can eventually adhere on the membrane surface even though the interaction energy at minimum separation distance is highly negative. The energy barriers significantly increase after incorporating sPSf in the membranes, while s-NIPS method does not give significant improvement (Fig. 7a). Similar interaction free energies trends were also found in a previous study (Wang et al., 2014), where the interaction energy between a PVDF membrane and sludge flocs (both surface charges are negative) also showed attractive LW and AB energies, a repulsive EL energy and a high energy barrier. Analogously, the interaction energy properties of the F-sNIPS membrane can approximately represent these of the patterned membranes as well.

3.4 CFD analysis of the flow regime near the membrane surface

A velocity path line profile near the membrane surface was obtained using CFD modeling (Fig. 8). The red color represents a higher velocity, and the blue color a lower. For patterned membranes, the velocity at the ridge region is higher than in the valley region, confirming the results in 3.2 that two different flows occurred near the membrane surface leading to a high-velocity on the ridge and a low-velocity in the valley. Small vortices were found in the bottom of the valley regions, which can alleviate microalgal cell deposition by mixing and scouring effects (Ma et al., 2015). A linear streamline is found near the flat membrane surface with a relatively low velocity, confirming a constant flow behavior. The results are in line with previous studies in which activated sludge particle and microalgal cells depositions were mitigated by using patterned membranes compared with the corresponding flat membranes under low *Re* number conditions (Lee et al., 2013; Zhao et al., 2020b).

A contour line profile was used to present the wall shear on the membrane surface (Fig. 9). The red color represents a higher wall shear, and the blue color a lower. With a higher wall shear, the fouling can be better alleviated (Du et al., 2017). Like the velocity profile, the wall shear at the ridge region is higher than in the valley region, confirming the results in 3.2 that an enhanced wall shear at the ridge region can give patterned membranes more channels to pass water. The wall shear on the flat membrane surface is too low to show, indicating that the wall shear on the flat membrane surface may be not high enough to remove the fouling, resulting in a serious cake layer on the flat membrane surface and a lower membrane flux. Similar results were found in previous studies, in which sludge particles and microalgal cells

were detached from the ridge of the patterned membranes with enhanced shear, while a flat membrane surface was fully covered by sludge and microalgal cells (Lee et al., 2013; Zhao et al., 2020b).

The CFD modeling clearly shows the advantage of using patterned membranes for harvesting microalgae. However, no significant difference is found between different pattern shapes, indicating that flow behavior may not be the main reason which influences the filtration performance.

Combing the results from 3.1 and 3.2, the patterns in the flow channel act as turbulence promotors, which can generate high velocity and wall shear on the ridge, and vortices in the valley. This can hinder microalgal cell attachment on the membrane surface, and in turn reduce fouling (Du et al., 2017). In addition, the wave patterns give a relatively larger un-fouled contact area in microalgal broth, which allowed more clean water to pass through, in turn resulting in a higher membrane flux and CP.

4. Conclusions

The effects of pattern shape on the morphology and filtration performance of negatively charged PSf membranes was investigated to harvest microalgal biomass. By adding sPSf to the PSf membrane, the hydrophilicity and surface charge were enhanced. In cross-flow filtration, all patterned membranes showed a higher CP, and wave-patterned membranes showed the highest CWP and flux in microalgal broths with 100% harvesting efficiency.

The mechanism of alleviating fouling for patterned membranes to harvest

microalgae was unraveled based on the membrane-cell interaction energy using the improved XDLVO theory, showing a higher repulsive energy when incorporating sPSf, thereby proving the fouling alleviating property of sPSf containing membranes. CFD modeling showed a higher velocity and shear stress on the apexes, indicating that the patterns can provide areas with less-fouling to allow more water passage.

Acknowledgements

Zhenyu Zhao acknowledges the China Scholarship Council for financial support.

Declaration of interests

The authors declare that they have no known competing financial interests or personal relationships that could have appeared to influence the work reported in this paper.

Reference

Ahmad, A.L., Mat Yasin, N.H., Derek, C.J.C. and Lim, J.K. 2013. Harvesting of microalgal biomass using MF membrane: Kinetic model, CDE model and extended DLVO theory. Journal of Membrane Science 446, 341-349.

Bilad, M.R., Mezohegyi, G., Declerck, P. and Vankelecom, I.F.J. 2012a. Novel magnetically induced membrane vibration (MMV) for fouling control in membrane bioreactors. Water Research 46(1), 63-72.

Bilad, M.R., Vandamme, D., Foubert, I., Muylaert, K. and Vankelecom, I.F.J. 2012b. Harvesting microalgal biomass using submerged microfiltration membranes. Bioresource Technology 111, 343-352.

Cao, H., Habimana, O., Semião, A.J.C., Allen, A., Heffernan, R. and Casey, E. 2015.

Understanding particle deposition kinetics on NF membranes: A focus on micro-beads and membrane interactions at different environmental conditions. Journal of Membrane Science 475, 367-375.

Chen, C., Zhao, Z., Ma, S., Rasool, M.A., Wang, L. and Zhang, J. 2020. Optimization of ultrasonic-assisted extraction, refinement and characterization of water-soluble polysaccharide from Dictyosphaerium sp. and evaluation of antioxidant activity in vitro. Journal of Food Measurement and Characterization 14(2), 963-977.

Choi, D.-C., Jung, S.-Y., Won, Y.-J., Jang, J.H., Lee, J.-W., Chae, H.-R., Lim, J., Ahn, K.H., Lee, S., Kim, J.-H., Park, P.-K. and Lee, C.-H. 2017. Effect of Pattern Shape on the Initial Deposition of Particles in the Aqueous Phase on Patterned Membranes during Crossflow Filtration. Environmental Science & Technology Letters 4(2), 66-70.

Derjaguin, B. 1934. Untersuchungen über die Reibung und Adhäsion, IV. Kolloid-Zeitschrift 69(2), 155-164.

Dobrak-Van Berlo, A., Vankelecom, I.F.J. and Van der Bruggen, B. 2011. Parameters determining transport mechanisms through unfilled and silicalite filled PDMS-based membranes and dense PI membranes in solvent resistant nanofiltration: Comparison with pervaporation. Journal of Membrane Science 374(1), 138-149.

Du, X., Wang, Y., Leslie, G., Li, G. and Liang, H. 2017. Shear stress in a pressure-driven membrane system and its impact on membrane fouling from a

hydrodynamic condition perspective: a review. Journal of Chemical Technology & Biotechnology 92(3), 463-478.

Gojkovic, Z., Shchukarev, A., Ramstedt, M. and Funk, C. 2020. Cryogenic X-ray photoelectron spectroscopy determines surface composition of algal cells and gives insights into their spontaneous sedimentation. Algal Research 47, 101836.

Heinz, O., Aghajani, M., Greenberg, A.R. and Ding, Y. 2018. Surface-patterning of polymeric membranes: fabrication and performance. Current Opinion in Chemical Engineering 20, 1-12.

Hoek, E.M.V. and Agarwal, G.K. 2006. Extended DLVO interactions between spherical particles and rough surfaces. Journal of Colloid and Interface Science 298(1), 50-58.

Hołda, A.K. and Vankelecom, I.F.J. 2015. Understanding and guiding the phase inversion process for synthesis of solvent resistant nanofiltration membranes. Journal of Applied Polymer Science 132(27).

Huang, R., Liu, Z., Yan, B., Li, Y., Li, H., Liu, D., Wang, P., Cui, F. and Shi, W. 2020. Layer-by-layer assembly of high negatively charged polycarbonate membranes with robust antifouling property for microalgae harvesting. Journal of Membrane Science 595, 117488.

Huang, W., Chu, H. and Dong, B. 2014. Understanding the fouling of algogenic organic matter in microfiltration using membrane–foulant interaction energy analysis: Effects of organic hydrophobicity. Colloids and Surfaces B:

Biointerfaces 122, 447-456.

Ilyas, A., Mertens, M., Oyaert, S. and Vankelecom, I.F.J. 2020. Synthesis of patterned PVDF ultrafiltration membranes: Spray-modified non-solvent induced phase separation. Journal of Membrane Science 612, 118383.

Jung, S.Y. and Ahn, K.H. 2019. Transport and deposition of colloidal particles on a patterned membrane surface: Effect of cross-flow velocity and the size ratio of particle to surface pattern. Journal of Membrane Science 572, 309-319.

Lau, A.K.S., Bilad, M.R., Nordin, N.A.H.M., Faungnawakij, K., Narkkun, T., Wang, D.K., Mahlia, T.M.I. and Jaafar, J. 2020. Effect of membrane properties on tilted panel performance of microalgae biomass filtration for biofuel feedstock. Renewable and Sustainable Energy Reviews 120, 109666.

Lee, Y.K., Won, Y.-J., Yoo, J.H., Ahn, K.H. and Lee, C.-H. 2013. Flow analysis and fouling on the patterned membrane surface. Journal of Membrane Science 427, 320-325.

Li, A., Zhang, L., Zhao, Z.-y., Ma, S.-s., Wang, M. and Liu, P.-h. 2016. Prescreening, identification and harvesting of microalgae with antibacterial activity. Biologia 71(10), 1111-1118.

Li, L., Wang, Z., Rietveld, L.C., Gao, N., Hu, J., Yin, D. and Yu, S. 2014. Comparison of the Effects of Extracellular and Intracellular Organic Matter Extracted From Microcystis aeruginosa on Ultrafiltration Membrane Fouling: Dynamics and Mechanisms. Environmental Science & Technology 48(24), 14549-14557.

Lin, H., Zhang, M., Mei, R., Chen, J. and Hong, H. 2014. A novel approach for quantitative evaluation of the physicochemical interactions between rough membrane surface and sludge foulants in a submerged membrane bioreactor. Bioresour Technol 171, 247-252.

Luo, L., Chung, T.-S., Weber, M., Staudt, C. and Maletzko, C. 2017. Molecular interaction between acidic sPPSU and basic HPEI polymers and its effects on membrane formation for ultrafiltration. Journal of Membrane Science 524, 33-42.

Ma, W., Rahaman, M.S. and Therien-Aubin, H. 2015. Controlling biofouling of reverse osmosis membranes through surface modification via grafting patterned polymer brushes. Journal of Water Reuse and Desalination 5(3), 326-334.

Manea, C. and Mulder, M. 2002. Characterization of polymer blends of polyethersulfone/sulfonated polysulfone and polyethersulfone/sulfonated polyetheretherketone for direct methanol fuel cell applications. Journal of Membrane Science 206(1), 443-453.

Marbelia, L., Bilad, M.R., Piassecka, A., Jishna, P.S., Naik, P.V. and Vankelecom, I.F.J. 2016a. Study of PVDF asymmetric membranes in a high-throughput membrane bioreactor (HT-MBR): Influence of phase inversion parameters and filtration performance. Separation and Purification Technology 162, 6-13.

Marbelia, L., Ilyas, A., Dierick, M., Qian, J., Achille, C., Ameloot, R. and Vankelecom, I.F.J. 2020. Preparation of patterned flat-sheet membranes using a

modified phase inversion process and advanced casting knife construction techniques. Journal of Membrane Science 597, 117621.

Marbelia, L., Mulier, M., Vandamme, D., Muylaert, K., Szymczyk, A. and Vankelecom, I.F.J. 2016b. Polyacrylonitrile membranes for microalgae filtration: Influence of porosity, surface charge and microalgae species on membrane fouling. Algal Research 19, 128-137.

Maruf, S.H., Greenberg, A.R., Pellegrino, J. and Ding, Y. 2014. Critical flux of surface-patterned ultrafiltration membranes during cross-flow filtration of colloidal particles. Journal of Membrane Science 471, 65-71.

Michels, M.H.A., van der Goot, A.J., Norsker, N.-H. and Wijffels, R.H. 2010. Effects of shear stress on the microalgae Chaetoceros muelleri. Bioprocess and Biosystems Engineering 33(8), 921-927.

Shahid, A., Malik, S., Zhu, H., Xu, J., Nawaz, M.Z., Nawaz, S., Asraful Alam, M. and Mehmood, M.A. 2020. Cultivating microalgae in wastewater for biomass production, pollutant removal, and atmospheric carbon mitigation; a review. Science of The Total Environment 704, 135303.

Song, D., Xu, J., Fu, Y., Xu, L. and Shan, B. 2016. Polysulfone/sulfonated polysulfone alloy membranes with an improved performance in processing mariculture wastewater. Chemical Engineering Journal 304, 882-889.

Sun, X., Wang, C., Tong, Y., Wang, W. and Wei, J. 2014. Microalgae filtration by UF membranes: influence of three membrane materials. Desalination and Water Treatment 52(28-30), 5229-5236.

Suparmaniam, U., Lam, M.K., Uemura, Y., Lim, J.W., Lee, K.T. and Shuit, S.H. 2019. Insights into the microalgae cultivation technology and harvesting process for biofuel production: A review. Renewable and Sustainable Energy Reviews 115, 109361.

van Oss, C.J. 1993. Acid—base interfacial interactions in aqueous media. Colloids and Surfaces A: Physicochemical and Engineering Aspects 78, 1-49.

Van Oss, C.J., Good, R.J. and Chaudhury, M.K. 1986. The role of van der Waals forces and hydrogen bonds in "hydrophobic interactions" between biopolymers and low energy surfaces. Journal of Colloid and Interface Science 111(2), 378-390.

Vandezande, P., Gevers, L.E.M., Weyens, N. and Vankelecom, I.F.J. 2009. Compositional Optimization of Polyimide-Based SEPPI Membranes Using a Genetic Algorithm and High-Throughput Techniques. Journal of Combinatorial Chemistry 11(2), 243-251.

Wang, F., Zhang, M., Peng, W., He, Y., Lin, H., Chen, J., Hong, H., Wang, A. and Yu, H. 2014. Effects of ionic strength on membrane fouling in a membrane bioreactor. Bioresour Technol 156, 35-41.

Zaouk, L., Massé, A., Bourseau, P., Taha, S., Rabiller-Baudry, M., Jubeau, S., Teychené, B., Pruvost, J. and Jaouen, P. 2018. Filterability of exopolysaccharides solutions from the red microalga Porphyridium cruentum by tangential filtration on a polymeric membrane. Environmental Technology, 1-18.

Zhao, F., Chu, H., Su, Y., Tan, X., Zhang, Y., Yang, L. and Zhou, X. 2016a. Microalgae harvesting by an axial vibration membrane: The mechanism of mitigating membrane fouling. Journal of Membrane Science 508, 127-135.

Zhao, Z., Cuellar Bermudez, S., Ilyas, A., Muylaert, K. and Vankelecom, I.F.J. 2020a. Optimization of negatively charged polysulfone membranes for concentration and purification of extracellular polysaccharides from Arthrospira platensis using the response surface methodology. Separation and Purification Technology 252, 117385.

Zhao, Z., Ilyas, A., Muylaert, K. and Vankelecom, I.F.J. 2020b. Optimization of patterned polysulfone membranes for microalgae harvesting. Bioresource Technology 309, 123367.

Zhao, Z., Li, Y., Muylaert, K. and Vankelecom, I.F.J. 2020c. Synergy between membrane filtration and flocculation for harvesting microalgae. Separation and Purification Technology 240, 116603.

Zhao, Z., Liu, B., Ilyas, A., Vanierschot, M., Muylaert, K. and Vankelecom, I.F.J. 2021. Harvesting microalgae using vibrating, negatively charged, patterned polysulfone membranes. Journal of Membrane Science 618, 118617.

Zhao, Z., Liu, P., Wang, S., Ma, S. and Cao, J. 2018. Combustion characteristics and kinetics of five tropic oilgal strains using thermogravimetric analysis. Journal of Thermal Analysis and Calorimetry 131(2), 1919-1931.

Zhao, Z., Ma, S., Li, A., Liu, P. and Wang, M. 2016b. Effects of Trophic Modes, Carbon Sources, and Salinity on the Cell Growth and Lipid Accumulation of

Tropic Ocean Oilgae Strain Desmodesmus sp. WC08. Applied Biochemistry and Biotechnology 180(3), 452-463.

Zhao, Z., Mertens, M., Li, Y., Muylaert, K. and Vankelecom, I.F.J. 2020d. A highly efficient and energy-saving magnetically induced membrane vibration system for harvesting microalgae. Bioresource Technology 300, 122688.

Zhao, Z., Rasool, M.A., Chen, C., Ma, S., Wang, L. and Huang, G. 2020e. Identification and screening of multiple tropical microalgal strains for antioxidant activity in vitro. Food Bioscience 36, 100649.

Zhong, P.S., Widjojo, N., Chung, T.-S., Weber, M. and Maletzko, C. 2012. Positively charged nanofiltration (NF) membranes via UV grafting on sulfonated polyphenylenesulfone (sPPSU) for effective removal of textile dyes from wastewater. Journal of Membrane Science 417-418, 52-60.

Zhu, X. and Jun Loh, X. 2015. Layer-by-layer assemblies for antibacterial applications. Biomaterials Science 3(12), 1505-1518.

Figures

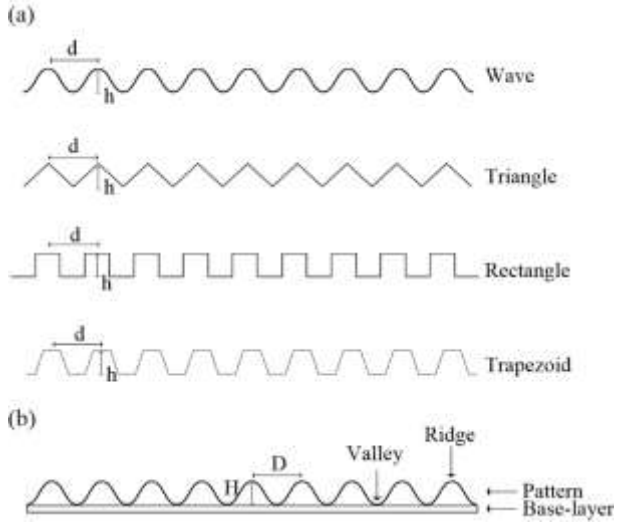

Fig. 1 Schematic diagram (a) of four different 3D-printed patterned knives cast with a 200 µm wet thickness as initial base-layer and (b) of the resulting patterned membrane.

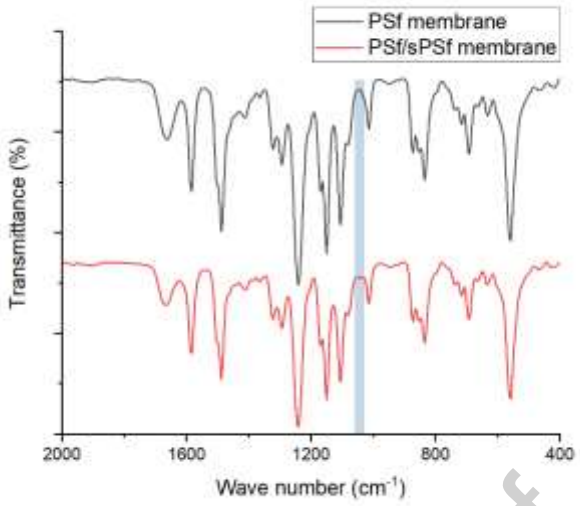

Fig. 2 FTIR spectrum of PSf and PSf/sPSf membranes. For clarification, the spectra were zoomed in from 400 to 2000 cm^{-1}.

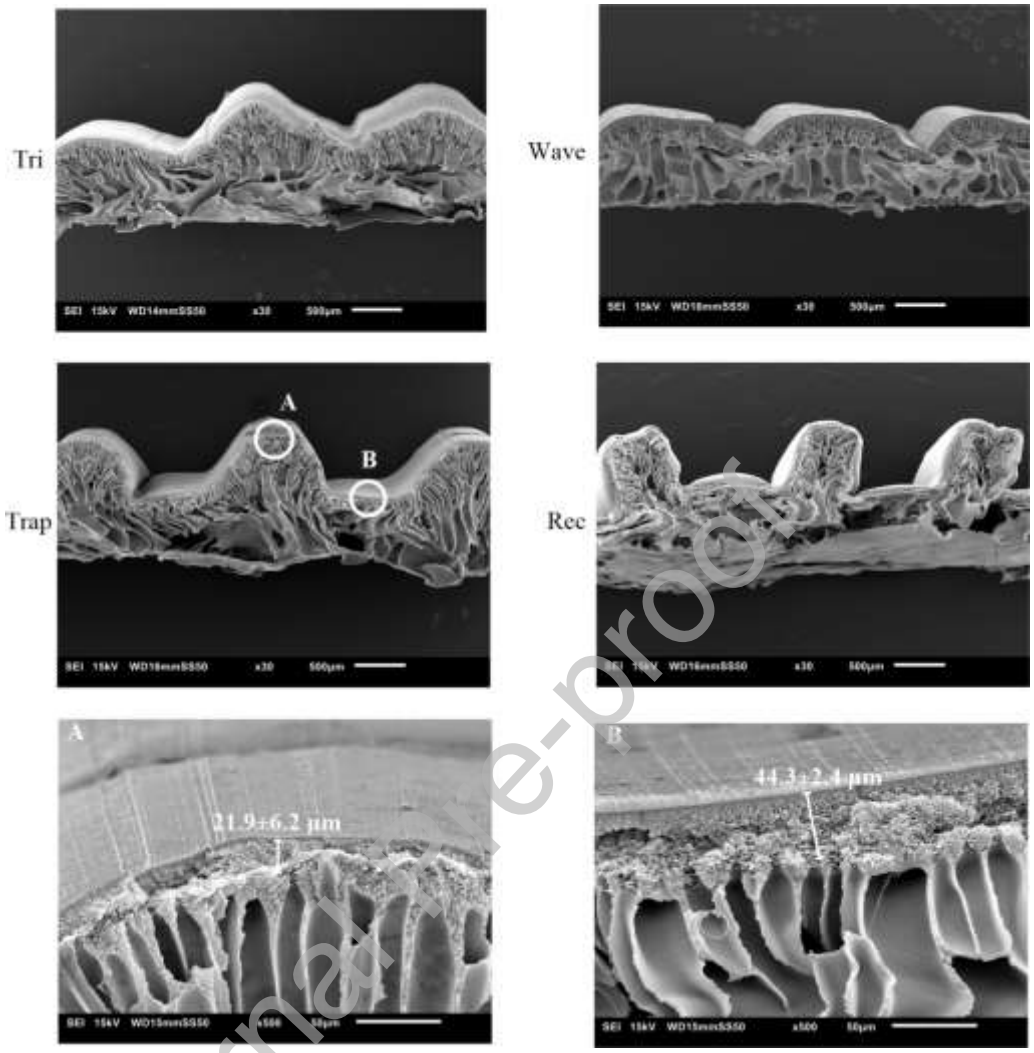

Fig. 3 Cross-sectional images of the patterned membranes prepared by different knife shapes. The close-ups below represent the pore structure (A) on the ridge and (B) in the valley of the pattern.

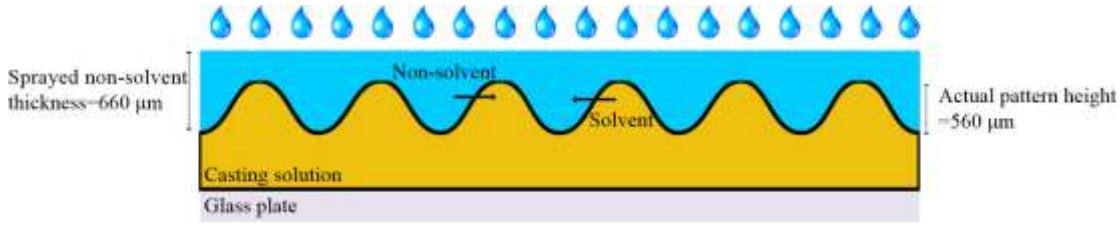

Fig. 4 Schematics of the non-solvent/solvent exchange during the s-NIPS process.

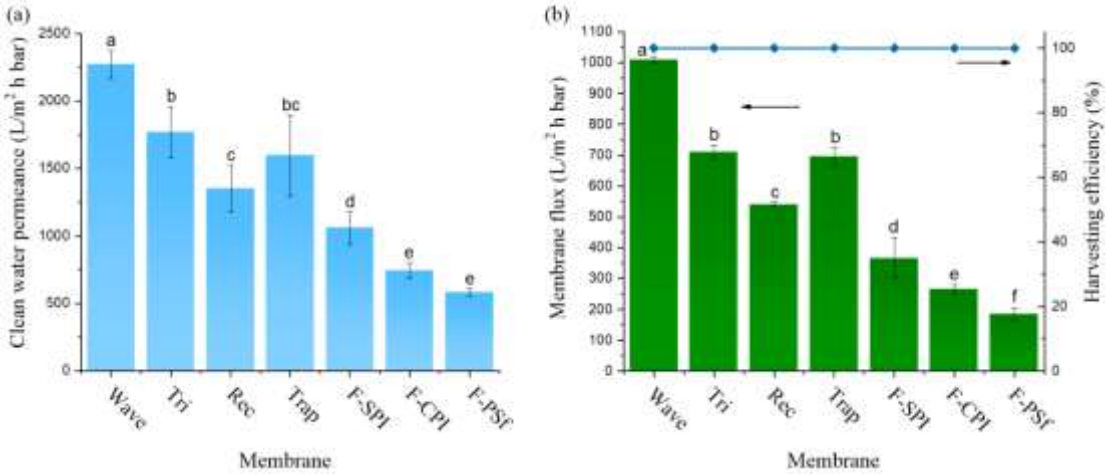

Fig. 5 (a) CWP, (b) membrane flux (using a microalgal broth as feed) and harvesting efficiency of the patterned and flat membranes in a dead-end filtration system.

***Note*: the different lower-case letters indicate results that are significantly (P<0.05) different. The line chart in (b) represents the harvesting efficiency and the bar chart represents the membrane flux.**

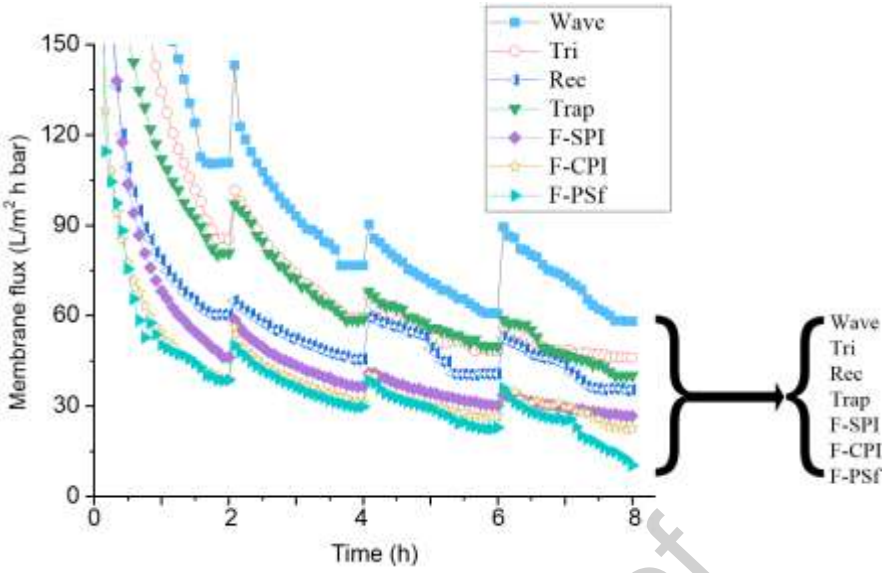

Fig. 6 Microalgal filtration using the stepwise method in a cross-flow system.

***Note*: to make the figure more readable, the figure only shows the membrane flux below 150 L/m^2 h.**

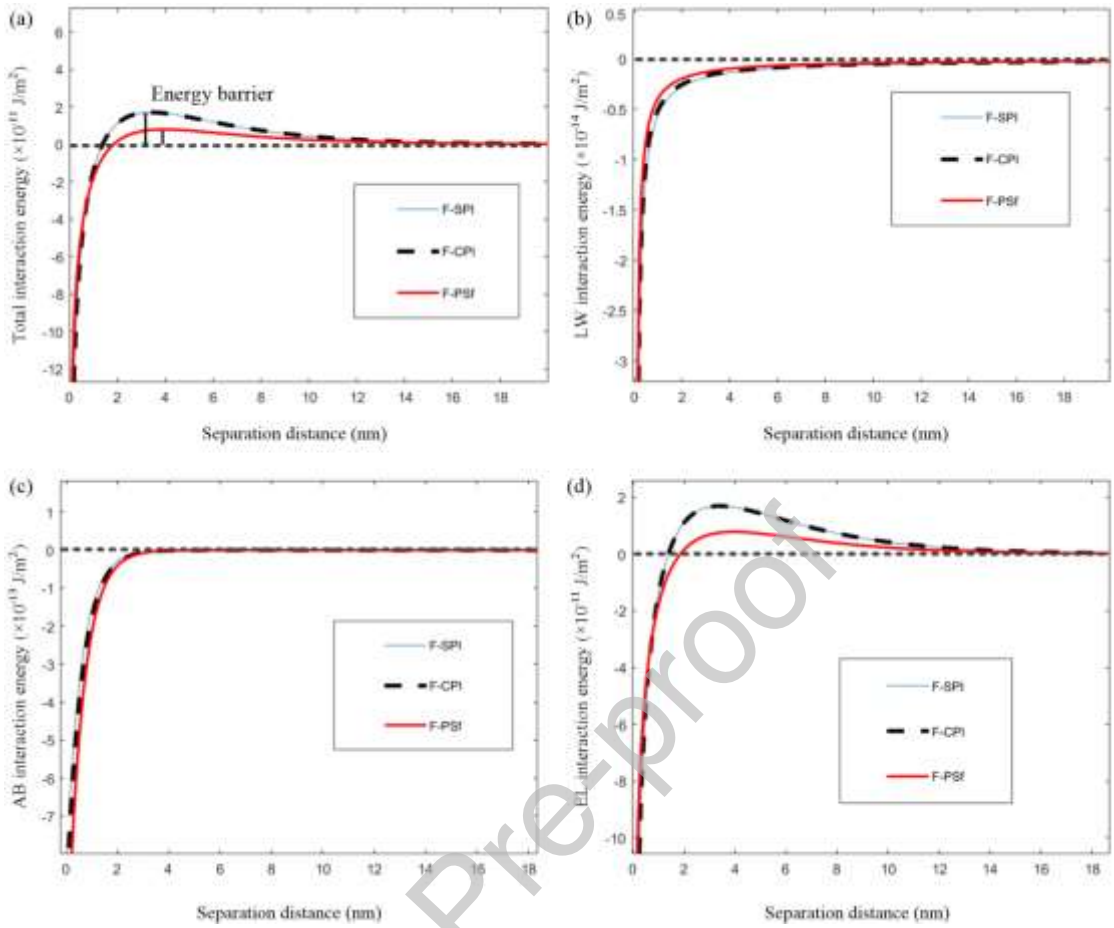

Fig. 7 Profiles of (a) total, (b) LW, (c) AB and (d) EL interaction free energies for membrane-microalgal cells combination as a function of the separation distance (the average microalgal cells radius is 6.1 μm).

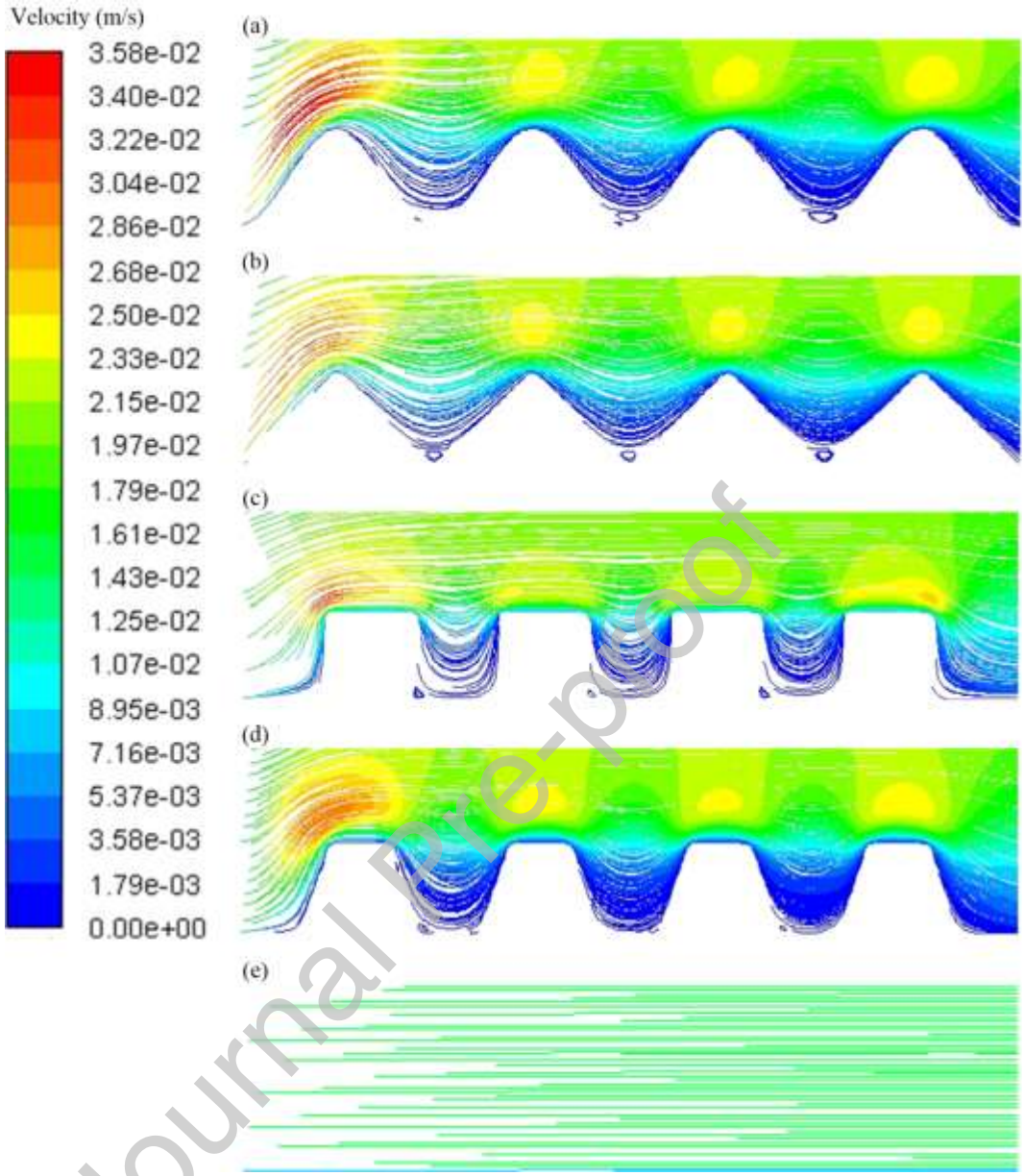

Fig. 8 Velocity streamline profiles simulated by CFD modeling for the (a) Wave, (b) Tri, (c) Rec, (d) Trap and (e) flat membranes at *Re*=109.

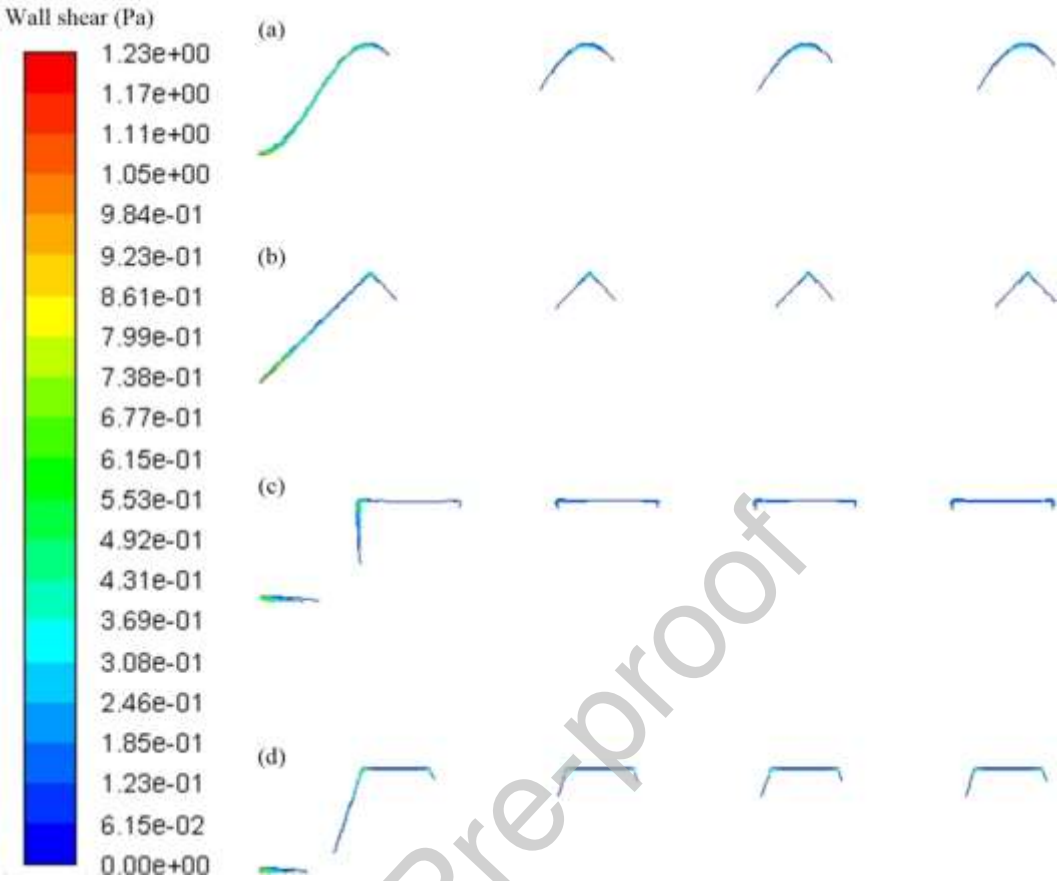

Fig. 9 Wall shear contour line profiles simulated by CFD modeling for (a) Wave, (b) Tri, (c) Rec and (d) Trap membranes at *Re*=109.

Note: the wall shear was too low to be shown for the flat membrane.

Tables

Table 1 Contact angle, zeta potential and surface tension data of membranes and *Desmodesmus* sp..

Sample	Contact angle (°)			Surface tension (mJ/m^2)					ZP (mV)
	θ_{wat} [a]	θ_{gly} [a]	θ_{dii} [a]	γ^{LW}	γ^-	γ^+	γ^{AB}	γ^{TOL}	
F-sNIPS	57.3±1.7	60.3±0.7	29.4±0.9	44.5	25.8	0.02	1.4	45.9	-95.8
F-NIPS	66.0±0.8	68.7±0.3	34.9±0.4	42.1	20.9	0.2	4.1	46.2	-95.8
F-PSf	86.0±0.8	88.7±0.3	44.9±0.4	37.1	11.0	1.5	8.1	45.2	-52.6
Algae	83.2±2.5	64.7±1.1	43.8±1.8	37.6	0.04	4.8	0.9	38.5	-18.0

[a] θ_{wat}, θ_{gly}, θ_{dii} are the contact angles determined using Milli-Q water, glycerol and diiodomethane, respectively.

Graphical abstract

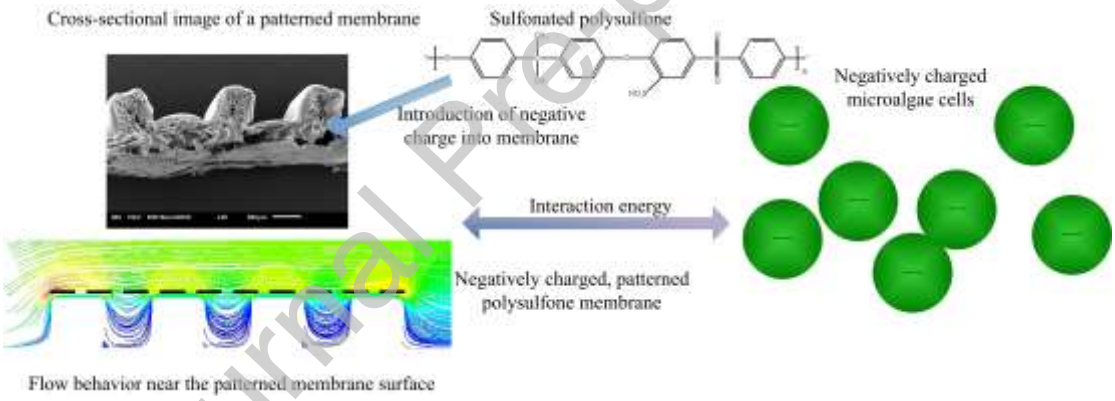

Table 2 Interfacial Gibbs free energies (mJ/m^2) at a minimum separation distance.

Sample	$\Delta G_{l_0}^{LW}$	$\Delta G_{l_0}^{AB}$	$\Delta G_{l_0}^{Tot}$
F-sNIPS	-5.8	-27.8	-33.6
F-NIPS	-5.3	-31.0	-36.3
F-PSf	-4.1	-38.7	-42.8
Algae	-4.3	-63.4	-67.7